JOURNAL OF SPACECRAFT AND ROCKETS
Vol. 31, No. 3, May–June 1994

Ablation Response Testing of Simulated Radioisotope Power Supplies

Steven A. Lutz* and Chris C. Chan*
Johns Hopkins University Applied Physics Laboratory, Laurel, Maryland 20723

Results of an experimental program to assess the aerothermal ablation response of simulated radioisotope power supplies are presented. Full-scale general purpose heat source, graphite impact shell, and lightweight radioisotope heater unit test articles are all tested without nuclear fuel in simulated reentry environments. Convective stagnation heating, stagnation pressure, stagnation surface temperature, surface recession profile, and weight loss measurements are obtained for diffusion-limited and sublimation ablation conditions. The recession profile and weight loss measurements show an effect of surface features on the stagnation face. The surface features alter the local heating which in turn affects the local ablation.

Nomenclature

A_s = surface area, mm^2
D = module diameter, mm
H_t = total enthalpy, MJ/kg
m = mass loss, g
P_{t2} = stagnation pressure behind the shock, atm
$q_{0,1}$ = stagnation heat flux for 0.3048-m-radius sphere, W/cm^2
s = module surface recession, mm
T_w = wall temperature, K
t = minimum aeroshell thickness, mm
X = vertical position with respect to nozzle center, mm
Y = horizontal position with respect to nozzle center, mm
ρ = ablating material density, g/cm^3

Subscripts

av = average
ref = reference
t = Total
w = wall

I. Introduction

THE Galileo spacecraft requires prolonged sources of electrical energy for the operation of the various system components. A radioisotope-fueled, thermoelectric generator is needed for this application. The radioisotope heat sources used in the Galileo spacecraft are the general purpose heat source (GPHS) and the lightweight radioisotope heater unit (LWRHU) shown in Figs. 1 and 2, respectively. All U.S. space missions involving a nuclear power source must be analyzed to assess the potential risk of the mission to the world's population and environment. An overview of the technical challenges of re-entry analysis of radioisotope heat sources is given by Lucero.[1] The present work provides an experimental database for evaluating the convective thermal and thermostructural response of the GPHS, LWRHU, and the graphite impact shell (GIS) (the component of the GPHS that houses the fueled clads) heat sources under accidental Earth re-entry conditions.

The ablation behavior of small graphite specimens is characterized by Lundell and Dickey.[2,3] The shape change of an ablating carbon-carbon nose tip is reported by Nestler.[4] The recession profiles over the external aeroshell of simulated radioisotope heat sources shown in Figs. 1 and 2 are of interest here.

The results of an experimental program designed to assess the ablation response of the full-scale, GPHS/GIS/LWRHU test articles (without the nuclear fuel) to simulated convective heating re-entry environments are presented. The re-entry conditions of interest include orbital decay and shallow-angle reentries where diffusion-limited oxidation and sublimation are the dominant ablation mechanisms, respectively. The primary measures of the test article response are the surface pressure, the surface temperature, and removal of the test article aeroshell material.

II. Experiment

The tests were conducted in the 20-MW Aerodynamic Heating Facility (AHF) and the 60-MW Interaction Heating Facility (IHF) arc heated tunnels at the NASA Ames Research Center. These arc tunnels are the only tunnels able to handle the large cross section of the GPHS test article while still delivering a re-entry simulation. The GPHS/GIS/LWRHU test articles are the components shown in Figs. 1 and 2 except the fueled clads and fuel pellets, which are replaced with a solid piece of ATJ graphite. The external aeroshell for the flight test articles is

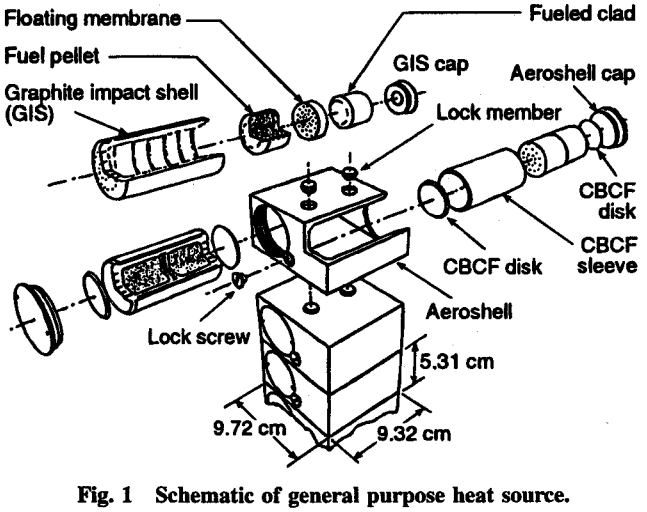

Fig. 1 Schematic of general purpose heat source.

Received Dec. 12, 1992; Presented as Paper 93-0381 at the AIAA 31st Aerospace Sciences Meeting, Reno, NV, Jan. 11–14, 1993; revision received Aug. 16, 1993; accepted for publication Aug. 17, 1993.

*Senior Professional Staff Engineer. Member AIAA.

Table 1 Summary of test conditions for the ablation response program at NASA Ames

FAC	Art./mat./geom.[a]	$q_{0,1}$, W/cm^2	P_{t2}, atm	H_t^b, MJ/kg	T_w, K
AHF	GIS/ATJ/*F*	104.55	0.110	14.89	2333
AHF	GIS/ATJ/*P*	104.25	0.110	14.89	2311
AHF	GIS/FWP/*F*	103.64	0.110	14.89	2364
AHF	GPHS/ATJ/*F*	72.34	0.057	14.89	1749
AHF	GPHS/ATJ/*P*	72.64	0.057	14.89	1701
AHF	GPHS/FWP/*F*	69.30	0.057	14.89	2084
AHF	RHU/FWP/*FE*	47.11	0.028	14.31	1851
IHF	GIS/ATJ/*F*	442.57	0.460	32.15	3350
IHF	GIS/ATJ/*P*	445.18	0.466	32.12	3300
IHF	GPHS/ATJ/*F*	570.60	1.014	27.91	—
IHF	GPHS/ATJ/*P*	569.47	1.000	28.05	—
IHF	GPHS/FWP/*F*	567.47	0.983	28.21	3600
IHF	RHU/FWP/*FE*	577.30	1.004	28.38	3300
IHF	RHU/FWP/*FS*	577.87	1.011	28.31	3800

[a]*F*—with surface features, *P*—Plain, *FE*—end-on, *FS*—side on.
[b]Estimated centerline value.

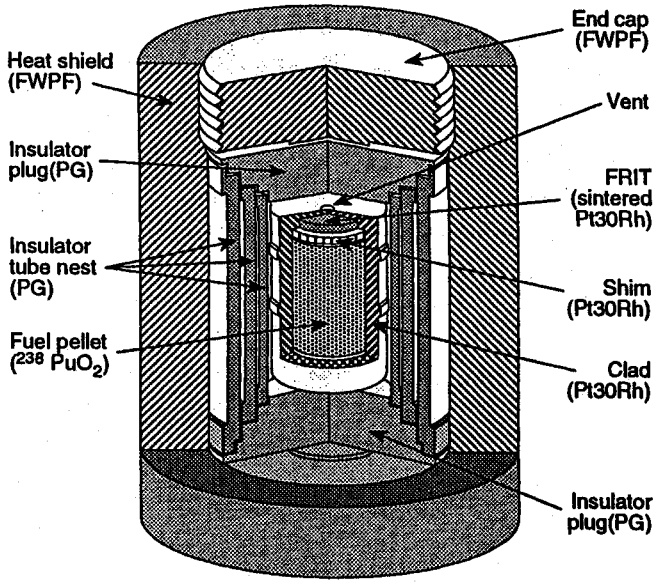

Fig. 2 Schematic of the lightweight radioisotope heater unit.

fabricated from Fine Weave Pierced Fabric (FWPF) Carbon-Carbon Material [Avco trademark]. Solid graphite (Union Carbide, TS-1792 ATJ) GPHS/GIS test articles with external dimensions identical to those shown in Fig. 1 are also tested as a reference ablation material. Graphite module holders are fabricated to attach the test articles to water-cooled stings. The GPHS test article is exposed with the broad face normal to the flow (broadface). The GIS/LWRHU test articles are exposed with the end cap normal to the flow (end-on). The LWRHU test article is also tested with the cylindrical surface normal to the flow (side-on). Water-cooled stagnation heating and pressure probes are used to characterize the arc jet. Pyrometers are used to record the surface temperature during the test. The test conditions are summarized in Table 1. The estimated percent uncertainties of the stagnation heating and pressure measurements are ± 10 % and ± 5 % in the AHF and ± 20 % and ± 10 % in the IHF, respectively. The estimated uncertainty of the pyrometer surface temperatures is ± 20 K for both facilities.

The test article ablation response is determined through surface recession and weight change measurements. The surface recession over the entire stagnation face is determined from the difference between the initial and post-test article height measured with a Brown and Sharp Model 7300 Validator Coordinate Measurement Machine. The estimated recession measurement uncertainty is ± 0.025 mm. The weight loss of the entire test article is determined from the difference between pre- and post-test measurements on an Arbor Model 5005 scale. The estimated weight measurement uncertainty is ± 0.02 *g*.

III. Model

Pretest predictions are required to determine the GPHS/GIS/LWRHU test article response to the arc jet tunnel conditions and size the instrumentation. The stagnation point recession and temperature are predicted with a specialized version (see Chan[5]) of the one-dimensional, transient conduction model, the Charring Material Thermal Response and Ablation Program (CMA) from Schoner.[6] Thermal grid networks for the GIS/LWRHU end-on models are constructed through the central axis of the test articles. The grid network for the GPHS model extended from the stagnation face aeroshell through the center of the GIS module to the backside aeroshell. The test articles are separated from their graphite holders by a small air gap and the conduction surface to the holder is minimal. Thus, the backside surfaces are assumed to be adiabatic. The stagnation heating of the flat-faced geometries is input as a correction factor to the stagnation heating of a 0.3048-m-radius sphere. The correction factor is the ratio of the flat-face-to-sphere velocity gradient parameter. The correction factors for the broadface GPHS, the end-on GIS, and the end-on LWRHU test articles are 1.700, 2.008, and 2.490, respectively. The correction factor does not account for the effect of the surface features on the heating. Model computations include the time required for the test article to reach the centerline position. The model gives the surface temperature and surface recession at each time step.

IV. Results

The centerline ablation response (along $X/X_{ref} = 0$) of the GPHS test article to the 20-MW AHF test conditions is shown in Fig. 3. The heating and pressure conditions are representative of what the test article would see in a broadface stable orbital decay re-entry. The test time is selected to give the same heat load (i.e., the integrated heat flux over the re-entry period) as a simulated orbital decay. The test time is initiated when the test article reaches the centerline position. The abscissa gives a dimensionless surface profile where the minimum thickness *t* is located along the housed GIS (i.e., within the GPHS aeroshell, Fig. 1) centerline. A comparison of a plain-face test article with the same external dimensions as one with surface features is shown. The surface profiles in the central portions of the article are nearly identical, indicating the repeatability of the tunnel conditions. Enhanced ablation is observed at the edges in the chamfer region of the features test articles. This enhanced ablation is also observed in the ATJ graphite test article mass loss measurements listed in the Fig. legend. The ablation is directly related to heating as noted by Putz and Bartlett.[7] The

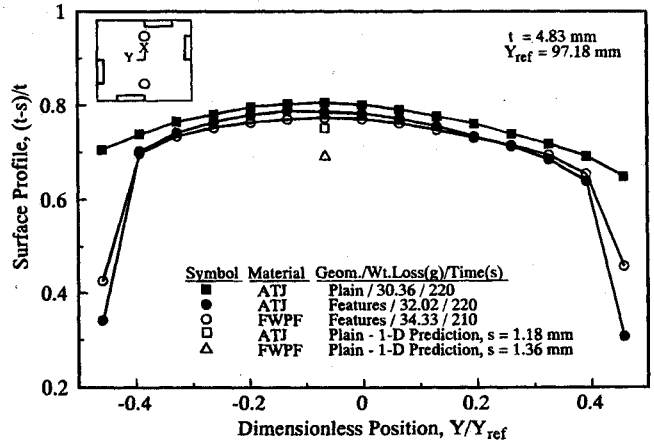

Fig. 3 Surface ablation profile (at $X/X_{ref} = 0$) of the GPHS test article at the 20-MW AHF test conditions.

corner flow augments the localized heating and results in a higher ablation there. Minimum recession occurs at the stagnation point and increases towards the edge of the test article. These profiles are consistent with the heating profiles on flat faced bodies reported by Marvin and Sinclair[3]: minimum at stagnation and increasing away from stagnation. The model overpredicts the stagnation point recession. The stagnation point (i.e., $X = 0.0$ mm and $Y = -6.35$ mm) is not located at the center of the module because the sting is deflected slightly by the tunnel flow.

The deflection of the sting is also observed for the centerline (along $X/X_{ref} = 0$) ablation response of the GPHS test article in the IHF shown in Fig. 4. The heating and pressure values are representative of a shallow-angle re-entry. The test times are selected to give a certain ablation fraction of the aeroshell. The minimum recession occurs at $X = 0.0$ mm and $Y = -25.4$ mm. The deflection is equivalent to an angle of attack of 1–2 deg. A comparison of the ATJ test articles shows a one-sided effect of the chamfer on the recession. Weight change measurements for the ATJ test articles confirm an effect of surface features on the ablation response. The second FWPF GPHS test article exposure recession shows a qualitatively similar ablation distribution, indicating the repeatability of the test conditions. The model overpredicts the stagnation point measurements.

A comparison of the GPHS test article ablation profiles along the opposing centerline bisector (along $Y/Y_{ref} = 0$) for both the AHF and IHF tests is shown in Fig. 5. In this orientation, the qualitative distribution of the IHF plain-face profile indicates only a slight effect of the sting deflection compared to the AHF plain-face profile. The lock recessed holes have a clear influence on the ablation profiles. These circular cavities have lower heating at the base resulting in the reduced ablation there. The chamfers are observed again to alter the local ablation.

The centerline surface profiles of the GIS test article for both the 20-MW and 60-MW tests are shown in Fig. 6. Here, the thickness t is referenced to as the minimum aeroshell cap thickness. The sting deflection for these tests is much less than the GPHS test article exposures because of the reduced frontal area. The IHF plain-face data are slightly skewed. The surface feature test article ablation profiles are flatter than the plain-face test article and show enhanced recession and weight loss. The model underpredicts the stagnation point ablation. The one-dimensional model is not an accurate representation of the test article. There is additional heating along the sides of the module.

The recession profiles for the LWRHU test article showed the same qualitative distribution as observed for the GIS test article. The stagnation point ablation measurements and predictions are summarized in Table 2. Once again, the predictions should be viewed with discretion because of the one-dimensional assumption.

V. Discussion

With the weight loss and recession measurements, it is possible to infer a qualitative distribution of mass loss over the entire test article. It would be expected that a majority of the mass loss should come from the stagnation face. An average mass loss from the stagnation face can be determined from

$$m_{av} = \rho A_s s_{av}$$

Referring to Fig. 3, an average value for $(t - s)/t$ is 0.75 and using the given equation yields $m_{av}/m_t = 0.62$ for the plain-face ATJ GPHS test article. Thus, 38 % of the mass loss ablated from the other GPHS test article faces in the AHF tests. A higher fraction ablates from the stagnation face for the 60-MW tests (Fig. 4): for $(t - s)/t = 0.65$, $m_{av}/m_t = 0.72$ for the ATJ plain-face test article. This trend is also observed for the GIS

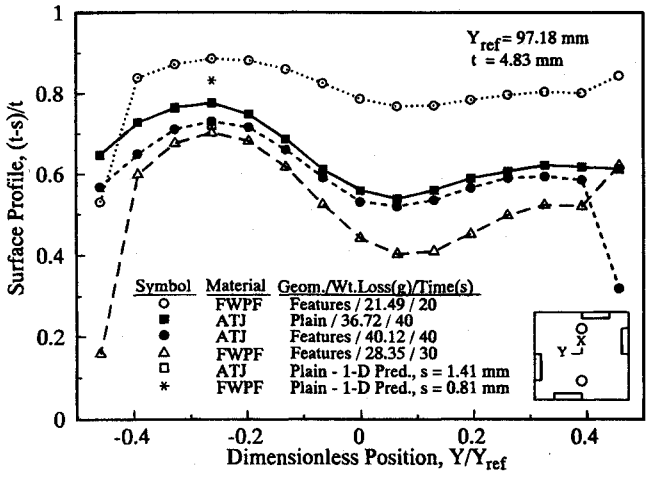

Fig. 4 Surface ablation profile (at $X/X_{ref} = 0$) of the GPHS test article at the 60-MW IHF test conditions.

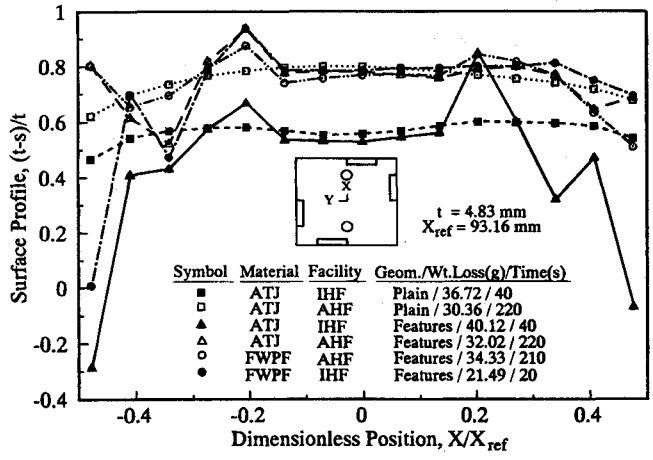

Fig. 5 Surface ablation profile (at $Y/Y_{ref} = 0$) of the GPHS test article at the 20-MW AHF and 60-MW IHF test conditions.

Table 2 Summary of stagnation point measurements and one-dimensional predictions for LWRHU test article

Fac./Geom.[a]	Time, s	Measured, mm	Predicted, mm
AHF/*E*	175	1.23	1.16
IHF/*E*	23	1.36	1.76
IHF/*S*	18	2.18	—

[a]*E*—end-on, *S*—side-on.

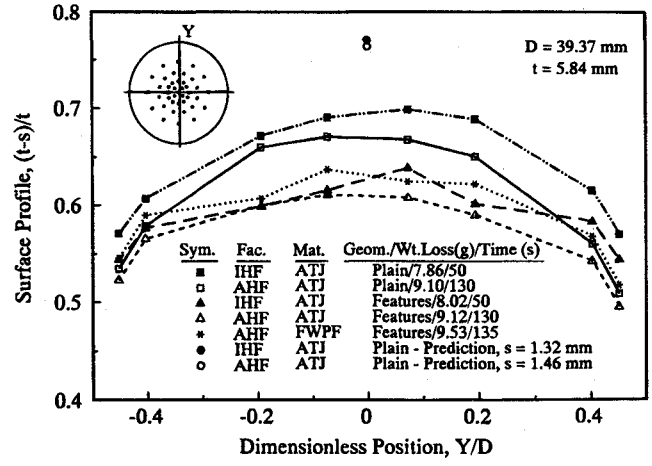

Fig. 6 Surface ablation profile of the GIS test article at the 20-MW AHF and 60-MW IHF test conditions.

test article, Fig. 6. For an average value for $(t - s)/t = 0.65$, $m_{av}/m_t = 0.47$ and 0.55 for the plain-face AHF and IHF GIS test articles, respectively. The GIS test article mass loss from the stagnation face is less than the GPHS test article because the surface is a smaller fraction of the total exposed area.

Surface features change the localized heating which, in turn, affect the local ablation on the stagnation face. The chamfer and lock recessed hole of the GPHS test article are regions where the heating is augmented and attenuated, respectively. The perforations in the GIS test article cap apparently alter the ablation distribution. The reduced mass of the cap due to the perforations must be accounted for to assess their effect on the ablation. The mass of ATJ material removed from the 41 perforations in the end cap is 0.56 g. This amount of mass reduces $(t - s)/t$ by 0.05. Reducing the ATJ plain cap GIS test article distributions in Fig. 6 by this amount brings them near the perforated cap profiles. The flatness in the perforated cap distribution may be attributed to the uniform distribution of the holes over a 23.5-mm diam.

VI. Concluding Remarks

The detailed surface recession measurements provide a clear picture of the ablation response of the stagnation face to fixed test conditions. The one-dimensional stagnation point prediction is good for the GPHS test article and well-insulated LWRHU test articles. End effects invalidate the one-dimensional approximation for the GIS test article prediction. The recession measurements clearly show the effects of the surface features on the local ablation.

Acknowledgments

The reported research was performed under Task ACA of Contract N00039-91-C-0001 with the Space and Naval Warfare Systems Command and was sponsored by and under the technical cognizance of the U. S. Department of Energy Office of Special Applications, R. G. Lange, Director. The authors acknowledge P. T. Brenza, D. W. Conn, E. F. Lucero, and J. C. Hagan (all from Johns Hopkins University Applied Physics Laboratory) for their contributions to this paper. The support of H. K. Tran, W. L. Love, and H. Goldstein of the NASA Ames Research Center and R. L. Zocher of the Los Alamos National Laboratory during the preparation and execution of the test program was greatly appreciated.

References

[1] Lucero, E. F., "Overview of Technical Challenges of Reentry Analysis of Radioisotope Heat Sources," AIAA Paper 93–0379, Jan. 1993.

[2] Lundell, J. H., and Dickey, R. R., "Ablation of Graphitic Materials in the Sublimation Regime," *AIAA Journal,* Vol. 13, No. 8, 1975, pp. 1079–1085.

[3] Lundell, J. H., and Dickey, R. R., "Ablation of ATJ Graphite at High Temperatures," *AIAA Journal,* Vol. 11, No. 2, 1973, pp. 216–222.

[4] Nestler, D. E., "High-Pressure Arc Test Performance of Carbon-Carbon Nose Tips," *Aerodynamic Heating and Thermal Protection Systems,* edited by L. S. Fletcher, Vol. 59, Progress in Astronautics and Aeronautics, AIAA, New York, 1978, pp. 351–367.

[5] Chan, C. C., "Modifications to the Aerotherm Charring Material Thermal Response and Ablation Program (CMA) for Carbon Ablation Analysis," Johns Hopkins Univ. Applied Physics Lab. Rept. TG-1373, Laurel, MD, March 1989.

[6] Schoner, R. J., "User's Manual, Aerotherm Charring Material Thermal Response and Ablation Program, Version 3," Aerotherm Rept. No. UM-70-14, AFRPL-TR-70-92, Mountain View, CA, April 1970.

[7] Putz, K. E., and Bartlett, E. P., "Heat-Transfer and Ablation-Rate Correlations for Re-entry Heatshield and Nosetip Applications," AIAA Paper 72–91, Jan. 1972.

[8] Marvin, J. G., and Sinclair, A. R., "Convective Heating in Regions of Large Favorable Pressure Gradient," *AIAA Journal,* Vol. 5, No. 11, 1967, pp. 1940–1948.

Michael E. Tauber
Associate Editor